# The Shear Response of Low Molecular Weight Poly(*n*-hexyl isocyanate) Wormlike Three-Arm Stars in Semidilute Solution

**Sanaul K. Siddiquee and Jan W. van Egmond***

*Department of Chemical Engineering, University of Massachusetts, Amherst, Massachusetts 01003*

*Received August 15, 1997; Revised Manuscript Received November 10, 1997*

ABSTRACT: The rheo-optical response to shearing of semidilute solutions of highly monodisperse, wormlike poly(*n*-hexyl isocyanate) three-arm stars was investigated using simultaneous birefringence and dichroism measurements. There were two modes to the birefringence response: a fast mode, corresponding to molecular orientation and a slow mode which, through scattering dichroism measurements, is confirmed to be associated with the dynamics of anisotropic multichain associations in solution. In addition, the dichroism measurements showed that these structures oriented perpendicular to the mean chain orientation within the structures. The optical equivalent of the shear stress, $n_{xy}$, scales as $(\dot{\gamma}c^{3.2})^{0.74}$ for these stiff, low molecular weight samples in the semidilute concentration regime.

## 1.0. Introduction

Recently, the effect of stiffness on chain dynamics and hence a solution's rheological response have been receiving increasing attention. Obviously, the stiffness of a polymer significantly alters its solution properties by influencing the polymer dynamics and chain interactions. Traditional studies have been limited to the two extremes of flexibility: the fully flexible chain and the rigid rod. The dynamic properties and rheological behavior of these two classes of polymers have been described in great detail theoretically.[1−5] However, there are a great many systems that fall between these two stiffness regimes. Hence, their dynamic and rheological responses are not adequately explained by these two cases. The first serious attempt to account for the effect of flexibility on solution dynamics is the Kratky−Porod wormlike chain that considers chain flexibility in dilute solutions.[6] The presence of a wormlike configuration and its effect on dilute solution properties have been confirmed by techniques such as static and dynamic light scattering. However, investigating the effect of flexibility in more concentrated solutions has been limited until recently by the lack of probing techniques suitable for moderate concentrations. Mechanical rheometry allows the measurement of bulk solution properties such as the viscosity, $\eta$, the storage modulus, $G'$ and the loss modulus, $G''$. However, it is notoriously difficult to obtain high quality data from mechanical rheometry of low viscosity solutions. Therefore, the effectiveness of mechanical techniques for investigating semidilute concentrations of polymers is severely restricted. Fortunately, the development of rheo-optical techniques has provided a useful avenue to study the shear response of solutions in this concentration range.[7−10]

Due to the well-characterized properties of poly(*n*-hexyl isocyanate) (PHIC),[11] this is expected to be a good polymer for studying the effect of flexibility on the solution dynamics of three-arm star polymers. Linear PHIC has been used repeatedly to evaluate theories on the behavior of wormlike chains in solution.[11−15] A previous rheo-optical study of linear PHIC has shown that concentration scaling of the shear response of the refractive index tensor, $n_{xy}$ is dependent on the chain flexibility.[16] While the chain stiffness is dependent on its persistence length, the overall chain flexibility is governed by the ratio of contour length to persistence length.[28] For short chains of nearly rodlike stiffness, $n_{xy}/\dot{\gamma} \sim c^{3.2}$. For longer, more flexible chains, the scaling relation becomes $n_{xy}/\dot{\gamma} \sim c^{4.2}$. This paper presents the effect of branching on the rheology of short chain PHIC by using a highly monodisperse sample consisting of star molecules of low arm molecular weight.

Previous investigations of linear PHIC have focused mainly on the liquid crystalline[17,18] and dilute concentration regimes.[11−14,17,19−21] Studies in the latter concentration regime have confirmed the wormlike conformation of PHIC and yielded important conformational parameters such as the radius of gyration, chain diameter, and the solution dependence of its persistence length.[11] Studies on linear PHIC and other semiflexible polymers have implied that they may form multi-chain associations in solution.[16,22−26] Static light scattering experiments show an increase in light intensity at low angles and additional "slow" modes are observed in dynamic light scattering experiments for some stiff polymers. Studies on the solution properties of PHIC stars have been limited due to the availability of polymer. To investigate whether three-arm PHIC stars associate in the semidilute concentration regime, dichroism measurements were conducted in conjunction with birefringence measurements. Birefringence measures the degree of orientation of the molecules within the sample during shear, while dichroism yields the degree of anisotropy of concentration fluctuations or multichain associations on the length scale of the probing light. More in-depth discussions of these techniques are available in the literature.[7−10,27]

## 2.0. Theory

A semi-flexible polymer obeying the Kratky−Porod model is usually termed a wormlike chain.[6,28] For these chains of intermediate stiffness, the equilibrium hydrodynamic solution properties differ substantially from those described by models for fully flexible polymers.[29] The flexibility of a polymer chain is dependent on the ratio of the contour length to the persistence length, $L/\alpha$, which decreases with increasing stiffness. A flexible linear polymer of $N$ Kuhn segments of length $a$ has a

S0024-9297(97)01236-9 CCC: $15.00 © 1998 American Chemical Society
Published on Web 04/03/1998

contour length $L = Na$ but an end to end distance considerably smaller than this. In the rodlike limit, the ratio of contour length to persistence length $L/\alpha \rightarrow 0$ and the end to end distance is equal to the contour length. In this rodlike limit, the viscosity and shear stress response are expected to scale with concentration as $c^3$.[3,16,30,31] As the ratio increases, the polymer chain passes through the wormlike regime, until the limit, $L/\alpha \rightarrow \infty$, at which point the polymer follows the same concentration scaling for the stress response as a flexible coil. Detailed studies with semidilute Xanthan solutions have shown that the viscosity scales with $c^3$ for $L/\alpha \cong 0.5$. The concentration scaling was found to increase with decreasing stiffness with $\eta \sim c^7$ for $L/\alpha \cong 10$.[30] Birefringence studies using linear PHIC showed $\eta \sim c^{3.2}$ for $L/\alpha \cong 0.8$, $\eta \sim c^{4.0}$ for $L/\alpha \cong 1.8$, and $\eta \sim c^{4.2}$ for $L/\alpha \cong 3.3$ in the semidilute regime.[16]

The shear response of polymer solutions is very dependent on the concentration. For monodisperse linear, rigid and wormlike polymers, four concentration regimes are discernible.[3] Below a critical concentration, $c^*$, the polymer dynamics are negligibly affected by adjacent chains. As the polymer concentration is increased beyond $c^*$, increasing topological constraints alter the solution dynamics resulting in highly correlated segmental fluctuations. The polymer dynamics are expected to be thus constrained at concentrations above which the average polymer separation is less than twice the radius of gyration of the polymer in solution. Therefore, the critical concentration at which the transition from the dilute to semidilute regime occurs is related to the root mean square radius of gyration, $\langle S^2\rangle^{1/2}$, by

$$c^* = \frac{M}{(4/3)\pi\langle S^2\rangle^{3/2} N_A} \tag{1}$$

where $M$ is the polymer molecular weight, $S$ is the radius of gyration of a single conformation and $N_A$ is Avagadro's number. For wormlike star polymers with arms of equal length, the mean square radius of gyration, $\langle S^2\rangle$, is estimated as[32]

$$\langle S^2\rangle_{star} = f^{-1}\alpha^2[(3f - 2)(L/3\alpha) + 2(1 - f) + 2(fx - 2x + 2)(\alpha/L) + x(x - 2)(\alpha/L)^2] \tag{2}$$

where $x = \exp(-L/\alpha)$, $f$ is the number of arms, $\alpha$ is the persistence length, and $L$ is the contour length of each arm. Equation 2 collapses to give the expression for a flexible star at the lower limit and a star with rodlike arms (but flexible core) at the higher limit.[32]

The transition between the semidilute and concentrated isotropic regimes is less clearly definable. For linear rodlike polymers, the transition to the concentrated isotropic regime is said to occur when the excluded volume interactions between the polymers are important for the solution's static properties as well as its dynamic properties. Thus on a microscopic (but not macroscopic) scale, there is a tendency for the polymer chains to order in concentrated isotropic solutions. For linear rods, the transition is estimated to occur when the rods are restricted to a mean space of size $bL^2$.[3] $b$ is the mean diameter of the tube formed by the constraint of adjacent chains. For linear wormlike chains of small contour length, the projected length of the chain on to the central segment: $L_e = 2\alpha[1 - \exp(-L/2\alpha)]$ is used instead of $L$.[33] Using these two approximations, a rough estimate of the transition between the semidilute and concentrated regimes, $c^+$, for linear wormlike chains is given by

$$c^+ = \frac{M/N_A}{4\alpha^2 b[1 - \exp(-L/2\alpha)]^2} \tag{3}$$

Undoubtedly, for wormlike star polymers, the extremely large volume exclusion at the branch point affects the the dynamics significantly. Since the arms of a star polymer are more correlated than adjacent linear polymers, the segmental density within the star polymer is expected to be higher. The result is that for the same molecular weight, $\langle S^2\rangle_{star} < \langle S^2\rangle_{linear}$ and the overlap concentration for the star polymer is greater than for a solution of an equivalent linear polymer. Therefore, the interpenetration required for the excluded volume interactions to significantly affect the static properties of the polymer in solution is expected to be greater. Hence $c^+_{star}$ will be greater than $c^+_{linear}$. However, how much greater is uncertain.

As the concentration is increased further, linear rodlike and wormlike polymers spontaneously orient on a macroscopic scale. Hence they are anisotropic even without the presence of an external orienting field.[3] This liquid crystalline phase is expected to occur also for wormlike star polymers with mobile cores.

This study is principally related to the investigation of the shear response of wormlike star polymers in the semidilute regime, with concentrations between $c^*$ and $c^+$.

## 3.0. Experimental Section

**3.1. Sample.** A very low polydispersity three arm PHIC sample was prepared by Professor Novak's group using living polymerization. A cyclohexane core is used to join the three arms together.[34] Cyclohexane adopts both "chair" and "boat" conformations and is able to switch between the two. Additionally, the bond between the cyclohexane core and PHIC chains is mobile but highly hindered. Therefore, though the star center cannot be considered freely jointed, a high degree of mobility is present at the star center. Tandem GPC/LS showed the polymer to have a molecular weight of $M_w = 44\,000$ (corresponding to each arm having a molecular weight of 14 600) and a polydispersity of 1.04. A fairly standard GPC/LS setup was used, consisting of an HP Series 1050 GPC in tandem with a Wyatt Technologies Dawn DSP1-F multidetector laser photometer and Wyatt/Opitlab 903 Interferometric refractometer. Tetrahydrofuran was used as a solvent. No GPC with respect to styrene standards was done on this sample. However, for other PHIC stars synthesized in the same manner, GPC with respect to styrene standards gave a polydispersity greater than 15. Previous light scattering measurements show that separation by molecular weight through the gel column for PHIC and other semiflexible polymers is relatively poor and results in a broad distribution of elution times which does not adequately represent the narrow polydispersity.[35] In addition, PHIC molecules have a much greater stiffness than polystyrene and hence a greater hydrodynamic radius in this range of molecular weights. Hence the usual method of evaluating molecular weight and polydispersity using GPC against three monodisperse polystyrene samples is inherently inaccurate for PHIC and other semiflexible polymers. Where separation due to differences in molecular weight is insufficient, a secondary technique such as light scattering is important to calculate the average molecular weight for each elution time.[36] In this manner, a more true representation of the polydispersity can be attained. Thus even if the polymer shows an affinity for the column which broadens the elution time distribution, an accurate

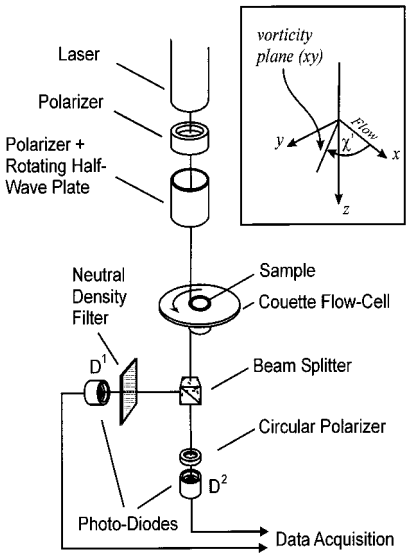


**Figure 1.** Optical train used in this study for the simultaneous measurement of birefringence and dichroism. The inset shows the coordinate system used with flow in the *x*-direction, the velocity gradient in the *y*-direction, and the *z*-axis being the direction that the laser beam is propagated.

measure of the weight average molecular weight and polydispersity is achieved with tandem GPC/LS.

There has only been limited study of the conformation of star shaped PHIC in solution. However, it is assumed that the arms of the star follow a similar length scaling and have the same solvent dependence as linear PHIC. Therefore, the conformation of the star polymer is expected to show the same unusual solvent dependence that has been observed with linear PHIC. Namely, the polymer dimensions decrease with increasing solvent polarity.[19,37] The decrease in the dimensions of the polymer is principly due to the reduction of the persistence length with increasing solvent dipole moment, $\mu_{solv}$.[38] The persistence length, α, has been estimated to be in the range 20−30 nm in TCE from $\mu_{TCE} = 1.32$ D.[38] The PHIC monomer has a molecular weight of 127 and a monomer projection length of 0.2 nm.[19] Using these values and a persistence length of 20 nm, $c^*$ is estimated to be 2.60 mg/cm$^3$ (0.163 wt %) from eq 1. For a linear polymer, the transition between the semidilute and concentrated regimes, $c^+_{linear}$, was estimated, using $b = 1.6$ nm,[11] as 9.3 wt % with eq 3. Since $c^+_{star}$ is expected to be greater than $c^+_{linear}$, a highest concentration of 15 wt % was used.

To prepare the 15 wt % solution, the polymer was dissolved at room temperature in 1,1,2,2-tetrachloroethane (TCE) and allowed to equilibrate for 3 days under continuous stirring. This solution was used as a stock solution and diluted to 12.6 wt %, 10.1 wt %, 7.5 wt %, 5.8 wt % and 2.8 wt % for the rheo-optical investigation. After each dilution, the solutions were allowed to equilibrate for at least 1 h prior to the experiment. TCE was chosen as the solvent for its relatively high viscosity and boiling point to ensure that evaporation remains minimal during the experiment. An additional reason for the choice of solvent was to allow comparison with previous experiments performed on linear PHIC in the same concentration regime.[16]

Repeating the same shear rate over the duration of the investigation showed no time dependent deviation of the birefringence, which implies that physical changes or evaporation during the course of the experiment remained insignificant and the solution had fully equilibrated prior to the experiment.

**3.2. Rheo-Optics.** The optical train used to measure the time dependent birefringence and dichroism response in the vorticity plane is shown in Figure 1. The light source was a 10 mW He−Ne laser of wavelength 632.8 nm. The intensity was controlled by a linear polarizer placed immediately after the laser. The polarization state generator (PSG) consisted of a second polarizer which was used to set the reference polarization angle followed by a half wave plate rotating at $\omega = 400$ Hz. After passing through the sample, a beam splitter divides the beam in two. For dichroism measurement, one beam is passed directly to detector D$^1$. The other beam is fed through a polarization state analyzer (PSA) consisting of a left hand circular polarizer to detector D$^2$ to register the effect of both birefringence and dichroism.

With the orientation angles of the birefringence, $\chi'$, and the dichroism, $\chi''$, being noncoaxial, the intensity at the detector D$^1$, $I^1$, is a function of $\chi''$ and the extinction of the primary dichroism axis, $\delta''$ [7,8]

$$\frac{I^1}{I^{10}} = 1 - \tanh \delta'' \cos 2\chi'' \cos 4\omega t - \tanh \delta'' \sin 2\chi'' \sin 4\omega t \quad (4)$$

where $I^{10}$ is the dc component of the intensity signal of the beam incident on the detector, D$^1$, and $\omega$ is the rotational frequency of the half-wave plate. The intensity at detector D$^2$, $I^2$, is dependent on $\chi'$, $\chi''$, the retardance $\delta'$ and the extinction $\delta''$

$$\frac{I^2}{I^{20}} = 1 - (\sin \delta' \sin 2\chi' + \tanh \delta'' \cos 2\chi'') \cos 4\omega t + (\sin \delta' \cos 2\chi' - \tanh \delta'' \sin 2\chi'')\sin 4\omega t \quad (5)$$

where $I^{20}$ is the dc component of the intensity signal of the beam incident on the detector, D$^2$. The retardance and orientation angle of the principle birefringence axis are then calculated to be

$$\delta' = \arcsin\{(R_1^2 - R_1^1)^2 + (R_2^2 - R_2^1)^2\}^{1/2} \quad (6)$$

$$\chi' = \frac{1}{2}\arctan\left(\frac{R_1^2 - R_1^1}{R_2^2 - R_2^1}\right) \quad (7)$$

where $R_1^1 = -\tanh \delta'' \cos 2\chi''$ and $R_1^2 = -(\sin \delta' \sin 2\chi' + \tanh \delta'' \cos 2\chi'')$ are the components of the intensities entering detectors D$^1$ and D$^2$ respectively that are in-phase with the polarized light exiting the rotating half wave plate. $R_2^1 = -\tanh \delta'' \sin 2\chi''$ and $R_2^2 = \sin \delta' \cos 2\chi' - \tanh \delta'' \sin 2\chi''$ are the out-of-phase components. Similarly, the extinction and orientation angle of the principle dichroism axis are given by

$$\delta'' = \operatorname{arctanh}\{(R_1^1)^2 + (R_2^1)^2\}^{1/2} \quad (8)$$

$$\chi'' = \frac{1}{2}\arctan\left(\frac{R_2^1}{R_1^1}\right) \quad (9)$$

The optical train was calibrated using a linear polarizer placed above the flow cell during calibration. Since an ideal polarizer has a retardance $\delta' = 0$ an extinction $\delta'' = -\infty$, an ideal polarizer oriented at 0° would yield both $R_1^1$ and $R_1^2$ equal to 1 while both $R_2^1$ and $R_2^2$ would equal 0. Therefore, using a linear polarizer as a standard optical element, the birefringence contributions of the elements that make up the optical train could be accounted for. Additionally, since the distortions of the polarization state of the beams exiting the beam splitter also appear as birefringence contributions, this is also accounted for by calibrating the optical train against a linear polarizer.

Obviously, in eqs 6 and 8, both $\sin \delta'$ and $\tanh \delta''$ are limited to less than or equal to 1. If the retardance exceeds $\pi/2$, $\sin \delta'$ starts to decrease—even though $\delta'$ continues to increase. In this case, birefringence is said to go "over orders". An example is shown schematically in Figure 2. In the first and third quadrants (where both $R'_1 = R_1^2 - R_1^1$ and $R'_2 = R_2^2 - R_2^1$ are the same sign), $\sin \delta'$ is positive and $\delta' = n\pi/2 + |\arcsin(\{R'^2_1 + R'^2_2\}^{1/2})|$. In the second and fourth quadrant (where $R'_1$ and $R'_2$ are different in sign), $\delta' = (n + 1)\pi/2 - |\arcsin$-

$(\{R'^2_1 + R'^2_2\}^{1/2})|$. Here $n$ is the number of orders (and complete quadrants) that $\delta'$ has passed through. Due to the flatness of the sin $\delta'$ curve as $\{R'^2_1 + R'^2_2\}^{1/2}$ approaches 1, the error in $\delta'$ increases sharply every time sin $\delta'$ approaches 1. Additionally, at very low values of $\{R'^2_1 + R'^2_2\}^{1/2}$, the relative error in sin $\delta'$ is increased. This is clearly seen with the highest concentration data presented in this paper and in ref 16.

The birefringence and dichroism are defined respectively as $\Delta n' = \delta'\lambda/2\pi d$ and $\Delta n'' = \delta''\lambda/2\pi d$, where $\lambda$ is the wavelength of the light passing through the sample, and $d$ is the pathlength through the sample. The birefringence, $\Delta n'$, is proportional to the anisotropy of the conformation tensor, $\langle rr \rangle$.[7] Therefore, the birefringence is a measure of the degree of orientation of the molecules within the sample. With this technique, we can study the response to shearing of the degree of alignment of the molecules in solution as well as the average angle of orientation, $\chi'$, to the flow direction.

If the shear stress is proportional to the $xy$-component of the conformation tensor, $\sigma_{xy} \propto \langle r_x r_y \rangle$, the stress optical rule holds.[7] This relates the birefringence anisotropy to the shear stress and the first normal stress difference. The stress optical rule has been shown to be true for most semidilute solutions of both rods and flexible coils.[5] However, the rule breaks down at high shear rates when the velocity gradient is sufficient to cause the polymer molecules to approach maximum alignment, resulting in saturation of the refractive index. Failure in the stress optical rule may also occur due to the presence of form contributions to the birefringence. Form birefringence arises when the solute and solvent refractive indices are sufficiently different and structures with length scales on the order of the wavelength of light are formed so that light is scattered anisotropically. If form contributions to the birefringence are present on the lengthscale of the probing light, the sample will exhibit form dichroism.[9] If the stress optical rule holds, the shear stress, $\sigma_{xy}$, and the first normal stress difference, $N_1$, are related to the birefringence anisotropy by the following expressions:

$$\sigma_{xy} = \frac{n_{xy}}{C} = \frac{\Delta n'}{2C} \sin 2\chi' \tag{10}$$

$$N_1 = \sigma_{xx} - \sigma_{yy} = \frac{\Delta n'}{C} \cos 2\chi' \tag{11}$$

$C$ is the stress-optical coefficient and $n_{xy}$ is the shear component of the refractive index tensor, $\mathbf{n}$.[10]

**3.3. Flow Cell.** An aluminum couette flow cell with a gap of 2 mm and outer rotating cylinder was used. The laser light propagated along the vorticity axis in the gap between the two cylinders and through two stationary flat quartz windows. An internal radius for the outer cylinder of 15.9 mm was sufficiently large to ensure a good approximation to homogeneous shear flow. The sample height (path length of the laser beam through the sample, $d$) was 19.1 mm. Shear rates from 0.05 to 200 $s^{-1}$ were used and the data were averaged over up to 20 identical runs to reduce experimental noise. Typically, averaging over 10 runs was sufficient. All experiments were conducted at room temperature (~21 °C).

## 4.0. Results and Discussion

Figure 3 shows the variation in the steady state birefringence with shear rate for solutions of three-arm PHIC star polymer of concentrations of 2.8, 5.8, 7.5, 10.1, 12.6, and 15.1 wt % in TCE. The strain units required to reach steady state was judged visually and appeared to be concentration dependent. For instance, at a concentration of 15 wt % and a shear rate of 1 $s^{-1}$, at least 15 strain units was needed. For a concentration of 5 wt % and a shear rate of 1 $s^{-1}$, steady state was reached faster than the sampling time of the equipment. At shear rates greater than 1 $s^{-1}$, the strain units required for steady state was independent of shear rate.

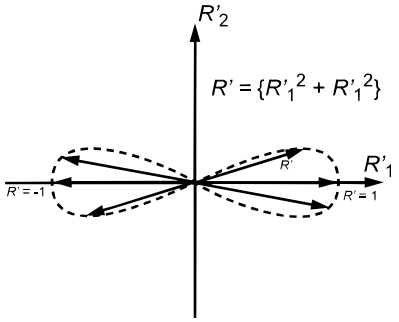


**Figure 2.** Schematic representation of $R'_1$ and $R'_2$ as $\delta'$ goes "over orders".

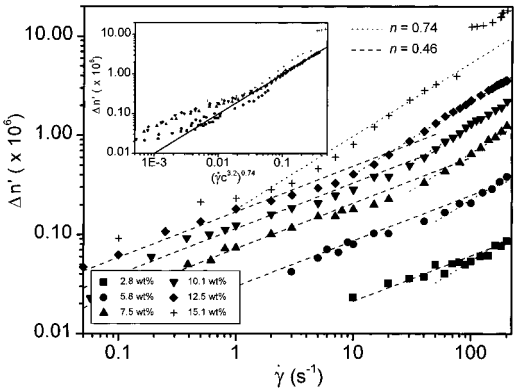


**Figure 3.** Variation of the steady state birefringence, $\Delta n'$, vs the shear rate, $\dot{\gamma}$, for the different concentrations studied is shown along with fits of $\Delta n' = A\dot{\gamma}^n$. The variation of steady state birefringence with $\dot{\gamma}c^{3.2}$ is shown in the inset.

However, at lower shear rates (where no overshoot was observed), less strain units were needed to reach steady state. The birefringence anisotropy shows two distinct regions. At low shear rates, $\dot{\gamma}$ less than ~30 $s^{-1}$, $\Delta n' \sim \dot{\gamma}^{0.46\pm0.04}$ while at high shear rates, $\Delta n' \sim \dot{\gamma}^{0.74\pm0.06}$. For the 15.1 wt % solution, $\Delta n'$ goes over orders while the 12.6 wt % solution at high shear rates approaches the limit for going over orders. The error at this limit leads to apparent high shear rate curvature in the steady state birefringence when plotted as a function of shear rate. It is seen in the inset to Figure 3 that, at high concentrations and shear rates, $\Delta n' \sim (\dot{\gamma}c^{3.2})^{0.74}$. The 15.1 wt % concentration is above this single power law dependency since it is close to the transition between the semidilute and concentrated solution regimes. At lower shear rates, the $(\dot{\gamma}c^{3.2})^{0.74}$ scaling underpredicts the birefringence for the higher concentrations. It is significant that this scaling is different from the $\Delta n' \sim \dot{\gamma}c^{3.2}$ relationship observed for linear PHIC of molecular weight 15 000, which is only slightly above the molecular weight of each arm.[16]

All of the concentrations exhibit shear-induced dichroism. Figure 4 shows the variation of the steady state dichroism, $\Delta n''$, with shear rate while the shear rate dependence of the birefringence and dichroism anisotropy for a single concentration (10.1 wt %) are displayed together in Figure 5. As with the birefringence, the steady state dichroism shows two shear rate dependent regimes. $\Delta n'' \sim \dot{\gamma}^{0.43\pm0.07}$ at low shear rates, and $\Delta n''$ appears to almost plateau with $\Delta n'' \sim \dot{\gamma}^{0.11\pm0.01}$ at higher shear rates. Thus both birefringence and dichroism have very similar power law behaviors in the low shear rate regime. As with the birefringence, the transition between the low and high shear rate dichroism regimes occurs at decreasing $\dot{\gamma}$ with increasing

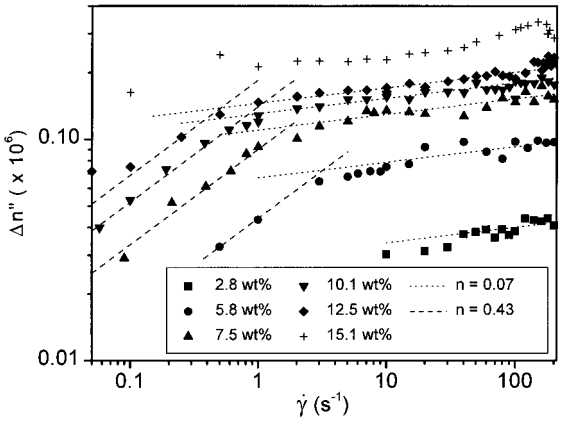


**Figure 4.** Variation of the steady state dichroism, $\Delta n''$, vs the shear rate, $\dot{\gamma}$, for the different concentrations studied.

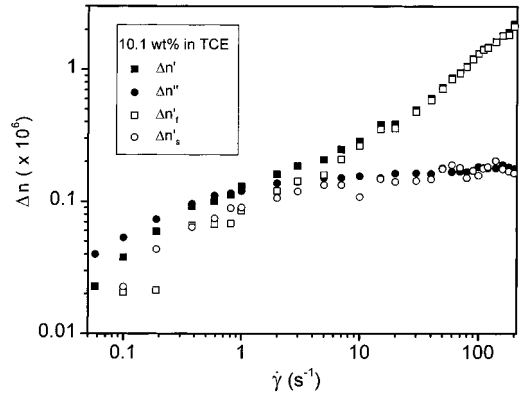


**Figure 5.** Comparison of the shear rate dependencies of the steady state fast mode birefringence, $\Delta n'_{fast}$, slow mode birefringence, $\Delta n'_{slow}$, the overall birefringence, $\Delta n'$ and the dichroism, $\Delta n''$ for the 10.1 wt % solution.

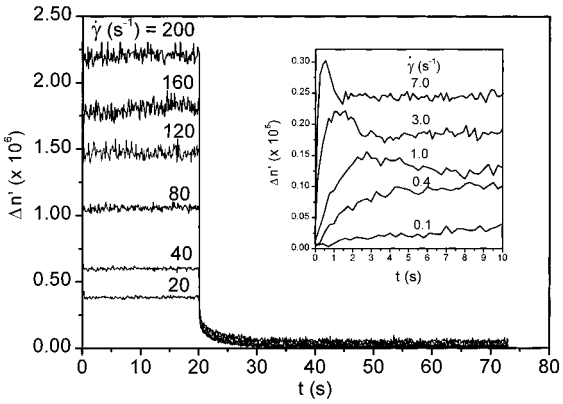


**Figure 6.** Time-dependent shear response of the birefringence anisotropy for the 10.1 wt % solution of PHIC. The inset shows the shear rate dependence of the startup transient overshoot.

concentration. This suggests that the birefringence and dichroism at low shear rates are due to related phenomena.

The time dependent response of the birefringence for the 10.1 wt % solution is shown in Figure 6. The behavior of the other concentrations is qualitatively similar with the steady state birefringence and relaxation times being concentration and shear rate dependent. The molecular relaxation of PHIC stars with short stiff arms in semidilute solution is very rapid. On the basis of the characteristic time of linear PHIC studied in our previous paper,[16] the molecular relaxation time for the stars studied here is expected to be in the range

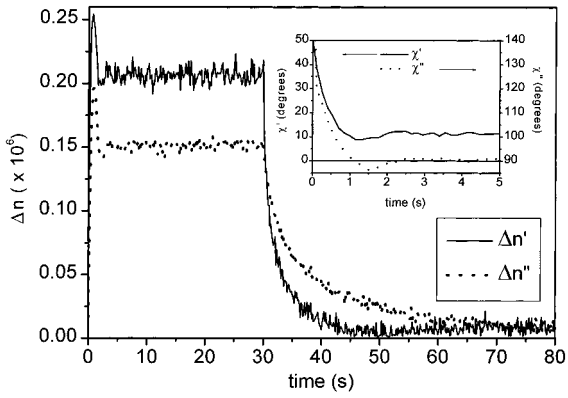


**Figure 7.** Comparison of transient behavior in the anisotropy for the 10.1 wt % solution at a shear rate of 5 $s^{-1}$. The inset is a comparison of the transient behavior in the orientation angle for the same solution at the same shear rate.

$t_{fast} \approx 0.1-10.0$ ms. For the higher shear rates, the birefringence reaches steady state almost immediately on flow inception at $t = 0$ s and is characterized by a fast relaxation mode on shear cessation ($t = 20$ s). In addition to the fast mode, a slow mode with relaxation time $t_{slow} \approx 5$ s is also visible. This unusual phenomenon was also noted in certain PHIC samples studied in our previous paper[16] and was attributed to the presence of large multichain structures.

The relative size of the overshoot after shear inception seen in the inset to Figure 6 increased with concentration. Its shear rate dependent characteristic time, $t_{peak}$, is faster than the sampling rate of the equipment at higher shear rates. $t_{peak}$ decreased with increasing shear rate such that the product $\dot{\gamma} t_{peak}$ remains constant at $3.43 \pm 0.34$, independent of concentration. For linear flexible polymers, the product $\dot{\gamma} t_{peak} \sim 2$ except at high strain rates[5] and the overshoot is due to chain overextension. For the PHIC samples studied here, chain over-extension is limited by the stiffness of these short chained polymers and their rigidity inhibits chain entanglement that would result in slower dynamics. For stars of such short arms in the semidilute regime, branching at the star center is unlikely to result in much additional entanglement. As with linear PHIC,[16] $t_{peak}$ is very much longer than the fastest relaxation time, $\tau_{fast}$, whose dynamics are associated with molecular orientation. The time dependent dichroism for the 10.1 wt % solution at a shear rate of 5 $s^{-1}$ is shown in Figure 7 simultaneously with the birefringence. The overshoot in the birefringence is hypothesized to be due to preexisting multichain structures in solution by closely following the dichroism overshoot. The amplitude of both overshoots increase with concentration and are barely visible for the 5.8 wt % solution. Hence, as with linear PHIC, the overshoot is likely due to preexisting multichain associations in solution. These aggregates appeared to be stable during shearing up to a shear rate of 200 $s^{-1}$. Rather, the overshoot is presumed to be due to collisions between adjacent structures during shearing. The presence of the aggregates was not thought to be related to sample preparation since the overshoots in the birefringence and dichroism were unaffected by the time the solutions were allowed to equilibrate during sample preparation.

Similar to linear PHIC,[16] the overall birefringence response is composed of two contributions. The fast mode has a relaxation time faster than the sampling rate, $\tau'_{fast} < 125$ ms since it is characterized by rapid

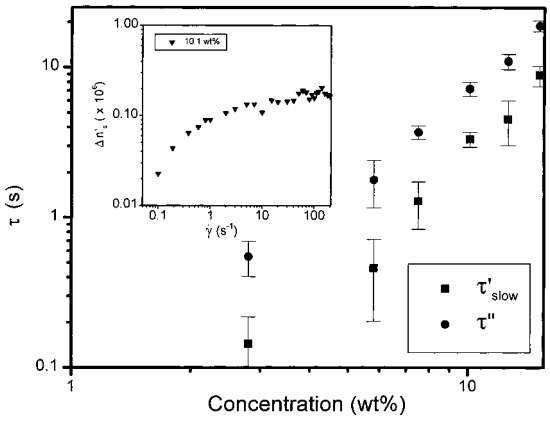


**Figure 8.** The variation of slow mode birefringence relaxation time, $\tau'_{slow}$, and the dichroism relaxation time, $\tau''$, with concentration. The inset shows the dependence of the steady state slow mode birefringence, $\Delta n'_{slow}$, on shear rate, $\dot{\gamma}$ for the 10.1 wt % solution.

relaxation though diffusion of individual chains.[3] Therefore, the slow mode relaxation time, $\tau'_{slow}$, can be found from $\Delta n'(t) = \Delta n'_0 + \Delta n'_s \exp[(t - t_1)/\tau'_{slow}]$. $\Delta n'_0$ is the baseline birefringence, $t_1$ is the time that shearing ceased and $\Delta n'_s$ is the initial size of the slow mode birefringence (when $t = t_1$). $\tau'_{slow}$ is independent of shear rate but is seen in Figure 8 to exhibit a power law dependence on concentration with $\tau'_{slow} \sim c^{2.80\pm0.29}$. The dichroism shows a single mode relaxation with $\tau'' \sim c^{2.47\pm0.16}$. This power dependence is only 13% different than the concentration dependence of $\tau'_{slow}$, suggesting a relationship between the two relaxation times.

The slow mode birefringence seen in the inset to Figure 8 has a bimodal dependence on shear rate with $\Delta n'_s \sim \dot{\gamma}^{0.48\pm0.06}$ at low shear rates and almost reaches a plateau with $\Delta n'_s \sim \dot{\gamma}^{0.10\pm0.02}$ at higher shear rates for all of the concentrations above 7.5 wt %. $\Delta n'_s$ was not estimated for the 2.8 and 5.8 wt % concentrations since the signal to noise ratio was of insufficient quality for accurate estimation of $\Delta n'_s$. The power law exponents are very similar to those for the steady state dichroism, which is further evidence that the slow mode is related to the orientation of multichain structures in solution.

In previous experiments on linear PHIC,[16] the slow mode in the birefringence was oriented in the flow direction at low concentrations and shear rates, where $\Delta n'$ is relatively small. At higher concentrations and shear rates the slow mode in $\Delta n'$ is surpressed. Unlike the solutions of star polymer, semidilute solutions of linear PHIC of molecular weight 34 000 were not found to be dichroic.[16] Dichroism measures anisotropy of structures on the length scale of the wavelength of the probing beam. Therefore, smaller length scale anisotropic associations may still be present for linear samples. The large excluded volume at the core of the three-arm PHIC molecules, in addition to the steric hindrance from branching, may limit how closely the chains can associate. Therefore, star PHIC is expected to form larger associations.

Two contributions to the birefringence explain the unusual shear rate response of the orientation angles. $\chi'$ and $\chi''$ are shown in the inset to Figure 7 to be 90° apart at the onset of shearing, with $\chi' \sim 45°$ and $\chi'' \sim 135°$. In the low shear rate regime, the slow mode birefringence rises more rapidly with increasing shear rate than the fast mode. Since the slow mode is governed by the dynamics of large structures, $\chi'$ is slow

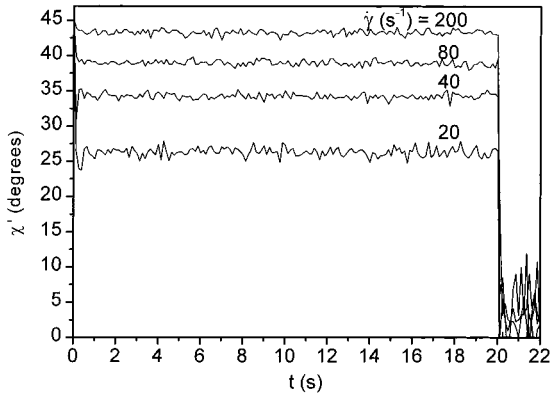


**Figure 9.** Transient response of the birefringence orientation angle, $\chi'$, at shear rates of $\dot{\gamma} = 20-200$ s$^{-1}$ for the 10.1 wt % solution.

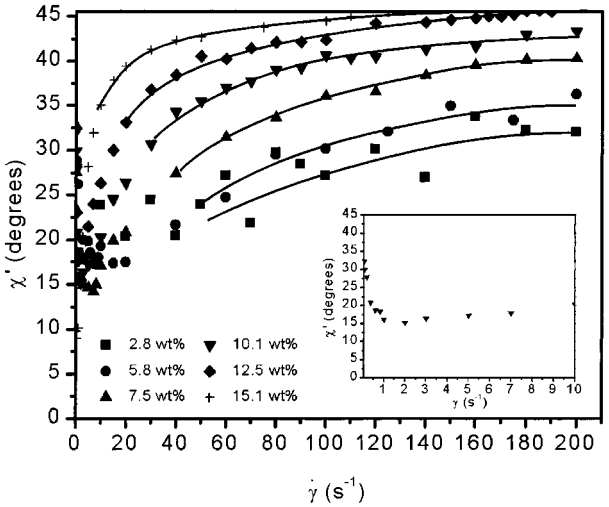


**Figure 10.** Shear rate, $\dot{\gamma}$, dependence of the steady state birefringence orientation angle, $\chi'$. The inset shows the shear rate dependence at low shear rates for the 10.1 wt % solution.

to achieve the steady state value, as seen in the inset to Figure 7. At higher shear rates ($\dot{\gamma} > 10$ s$^{-1}$) when the slow mode has plateaued, the solution dynamics are dominated by the fast mode and the steady state orientation is reached rapidly, as observed in Figure 9. As $\chi''$ drops to 90°, the slow mode remains approximately perpendicular to the dichroism and the overall $\chi'$ settles at a compromise angle governed by the fast and slow contributions. $\chi'$ drops immediately to 0° after shear cessation due to the rapid fast mode relaxation. The overall birefringence orientation angle is then governed only by the slow mode, which disorients relatively slowly.

In Figure 10, the steady state $\chi'$ approaches 45° as $\dot{\gamma} \rightarrow 0$ since the slow mode is oriented at 45°. Initially, the overall steady state birefringence orientation angle tends toward the flow direction as the shear rate is raised and the slow mode birefringence, which orients along the flow axis with increasing shear rate, rises more quickly than the fast mode. However, above a certain shear rate ($\dot{\gamma} \sim 10$ s$^{-1}$), the amplitude of the slow mode plateaus while the fast mode contribution continues to rise rapidly. Hence, at the high shear rates where the solution behavior is dominated by molecular dynamics, the steady state $\chi'$ approaches 45°. For typical polymers, $\chi' \rightarrow 45°$ as $\dot{\gamma}\tau_{fast} \rightarrow 0$ since the Newtonian limit is reached. Entanglements cause flexible chains to align increasingly towards the flow

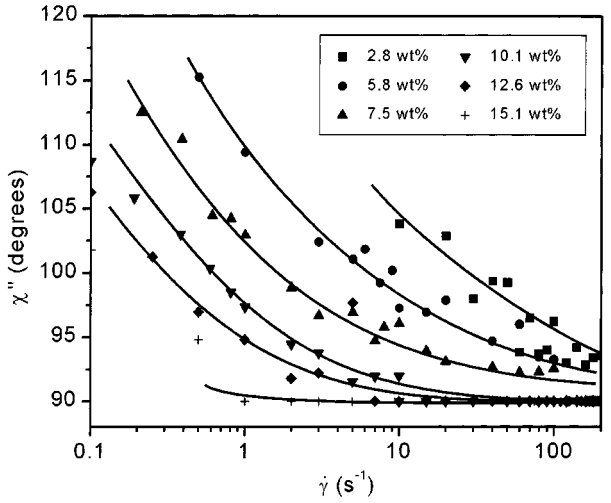


**Figure 11.** Shear rate, $\dot{\gamma}$, dependence of the steady state dichroism orientation angle, $\chi''$.

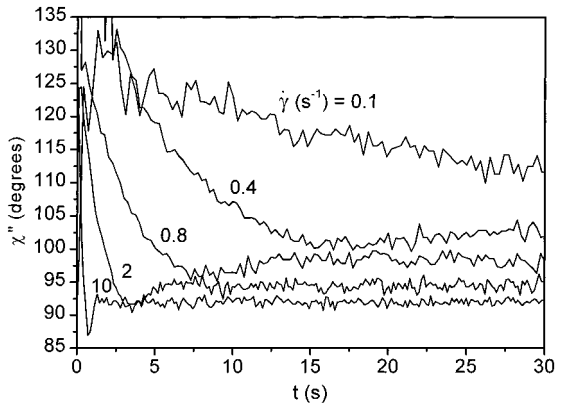


**Figure 12.** Response of the dichroism orientation angle at low shear rates ($\dot{\gamma} = 0.1-10.0$ s$^{-1}$) for the 10.1 wt % solution shows the shear dependence of the transience in the dichroism orientation angle.

axis as the solution is sheared at higher rates. Entanglements are insignificant for short and stiff wormlike polymers in the semidilute regime at the shear rates probed in this work, and interchain interactions are extremely rapid. Hence the orientation angle would be expected to remain at the newtonian limit of 45° if no slow mode were present.

Figure 11 shows the steady state orientation of the dichroism. The steady state $\chi''$ approaches 135° at extremely low shear rates and tends to 90° as the shear rate increases. The higher the concentration, the lower the shear rate at which an orientation of 90° is reached by the dichroism. The transient behavior shown in Figure 12 for the 10.1 wt % solution confirms that at extremely low shear rates, $\chi''$ is oriented at 135° at small times. Comparison of $\chi''$ and the slow mode birefringence suggests the presence of anisotropic chain associations whose major axes are perpendicular to the orientation of the chains within these associations. This is represented in Figure 14. For the higher concentrations after shear cessation, the dichroism orientation angle relaxes slowly due to the size of the associations and interactions with their neighbors. At the lower concentrations, the disorientation of the associations is much more rapid. In addition, little overshoot in the dichroism is observed with time for the 5.8 or 2.8 wt % solutions (data not shown) since the associations are small at these concentrations, resulting in less interaction between adjacent associations and faster dynamics. From the behavior of the dichroism, we believe that these multichain associations are not shear induced but are present at all times. Prior to shearing, they are randomly oriented. The application of a shear field aligns these associations, increasing both the dichroism and the slow mode birefringence. When maximum orientation of the associations is achieved, the shear rate dependence of the dichroism and slow mode birefringence drops significantly.

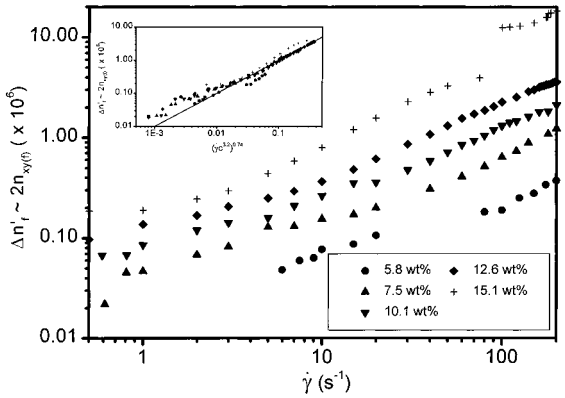


**Figure 13.** Dependence of the steady state fast mode birefringence anisotropy, $\Delta n'_f$, on shear rate, $\dot{\gamma}$, for concentrations of 5.8−15.1 wt %. $\Delta n'_f$ is plotted against $(\dot{\gamma}c^{3.2})^{0.74}$ in the inset.

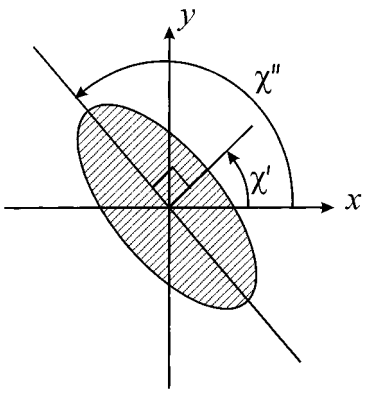


**Figure 14.** Representation of a multichain association with the major dichroism axis oriented perpendicular to the major birefringence axis.

These experimental results cannot conclusively determine the nature of the associations in solution or explain why they occur. Solvent effects may play an important part. PHIC, a "hairy" wormlike polymer, is soluble in a very limited number of solvents. If TCE is a poor solvent, the PHIC chains would prefer to associate.[3] The local polymer density may be sufficiently high to approach the concentrated solution regime. Then the local concentration would result in microscopic ordering within these associations even without the application of a shear field. Another possible reason which has been discussed in our previous paper is the presence of electrostatic molecular attraction[16] between the delocalized $\pi$-bonds of adjacent molecules which may be sufficiently strong to cause adjacent molecules to group together.

As with solutions of linear PHIC,[16] the response of the overall birefringence anisotropy and orientation angle to shearing is governed by two non-coaxial modes. Additional insight into each mode is gained by decoupling the slow mode from the fast mode. To a first approximation, the overall refractive index tensor, **n**,

is the sum of the refractive index tensor for the slow mode, $\mathbf{n_s}$ and for the fast mode, $\mathbf{n_f}$. The overall birefringence anisotropy and orientation angle are then related to these fast and slow contributions by eqs 12 and 13. Since the interchain interactions which account

$$\Delta n'^2 = \Delta n'_f{}^2 + \Delta n'_s{}^2 + 2\Delta n'_f \Delta n'_s \cos[2(\chi'_s - \chi'_f)] \quad (12)$$

$$\tan(2\chi') = \frac{\Delta n'_s \sin(2\chi'_s) + \Delta n'_f \sin(2\chi'_f)}{\Delta n'_s \cos(2\chi'_s) + \Delta n'_f \cos(2\chi'_f)} \quad (13)$$

for the fast mode are extremely rapid, $\chi'_f \sim 45°$ is a good approximation. $\Delta n'_s$ has been estimated previously by interpolating the slow mode relaxation back to the steady state value. Since both $\Delta n'$ and $\chi'$ are known, the fast mode birefringence, $\Delta n'_f$, and the orientation of the slow mode, $\chi'_s$, could be estimated. $\Delta n'_f$ is plotted against $\dot\gamma$ and $(\dot\gamma c^{3.2})^{0.74}$ in Figure 13 for the solutions of star PHIC. It is evident in Figures 5 and 13 that the importance of the slow mode on the steady state birefringence is limited to lower shear rates. $\Delta n'_f$ deviates less from the power law dependence on $(\dot\gamma c^{3.2})^{0.74}$ at higher shear rates where $\Delta n'_f \sim \Delta n'$. In Figure 3, little deviation of the steady state $\Delta n'$ from the single power dependence on $(\dot\gamma c^{3.2})^{0.74}$ is observed for the 2.8 and 5.8 wt % solutions. The small size of the associations in solution at these lower concentrations results in minimal interactions between the associations during and after shear.

The stress optical rule breaks down when there are multiple contributions to the shear birefringence and when large lengthscale structures are present.[7] Therefore, eqs 10 and 11 do not hold when the overall birefringence, $\Delta n'$, is used. However, the most important contribution to the stress is the shear response of the molecular orientation and alignment. Therefore, defining $n_{xy(f)}$ as the shear component of $\mathbf{n_f}$, $n_{xy(f)}$ is related to the fast mode birefringence by $n_{xy(f)} \approx \Delta n'_f/2$ since $\sin(2\chi'_f) \sim 1$. Then the optical equivalent of the shear stress also scales with concentration as $n_{xy(f)} \sim (\dot\gamma c^{3.2})^{0.74}$. This is significant since in our previous paper, $n_{xy}$ was shown to scale as $\dot\gamma c^{3.2}$ for linear PHIC of molecular weight 15 000, which is similar to the molecular weight of the star arms.[16] The concentration scaling of the shear response of PHIC stars is dependent on the molecular weight of each arm since the concentration dependence is related to the chain flexibility. The differences in the scalings between the linear and star samples maybe due to the star's mobile center as well the additional arm since there are no other major differences between the two samples.

There are other differences between the shear response of linear PHIC and the three armed stars studied here. For the linear PHIC samples, Figure 15 shows the linear dependence of the fast mode birefringence on shear rate. A much weaker, nonlinear, $\Delta n'_f \sim \dot\gamma^{0.74\pm0.06}$ dependence was observed for the star PHIC solutions, and there is no evidence of a linear viscoelasticity regime which is observed for most polymer solutions at low values of $\dot\gamma\tau_r$ where $\tau_r$ is the longest relaxation time of the solution.[5] Additionally, the star polymer exhibits less birefringence than the linear sample of molecular weight 34 000 (roughly equivalent to two of the star arms) since the mobile core and third arm reduce the overall degree of orientation but is more birefringent than a similarly concentrated solution of linear PHIC of molecular weight 15 000 (roughly equivalent to each star arm).

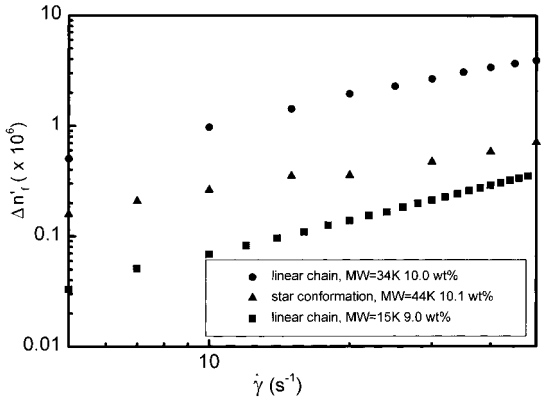


**Figure 15.** Comparison of the shear response of $\Delta n'_f$ for the 10.1 wt % star polymer solution with $\Delta n'$ for a 9.0 wt % solution of linear PHIC in TCE of molecular weight 14 000 and a 10.0 wt % solution of linear PHIC in TCE of molecular weight 34 000.

## 5.0. Conclusions

There are two distinctive contributions to the overall molecular alignment and orientation. The very rapid molecular dynamics result in a fast mode. The shear component of the refractive index tensor for the fast mode, $n_{xy(f)}$, scales as $(\dot\gamma c^{3.2})^{0.74}$ for PHIC stars of molecular weight 44 000 in the semidilute regime. The orientation of the fast mode birefringence, $\chi'_f \approx 45°$, is similar to that observed with linear PHIC. However, unlike linear PHIC, $n_{xy(f)}$ does not exhibit a linear dependence on shear rate. The slow mode is due to the existence of anisotropic associations which orient in a shear field. The major axis of these associations are perpendicular to the mean orientation of the component molecules and tend to orient perpendicular to the flow axis at high shear rates.

**Acknowledgment.** The authors gratefully acknowledge the financial support provided by the NSF/MRSEC program at the University of Massachusetts under Grant NSF/DMR-9400488 and a Faculty Research Grant (FRG) at the University of Massachusetts. We express our appreciation to Professor Bruce Novak and Susanne Hoff for developing the innovative reaction processes necessary to produce these samples and to Nathan Jones for their preparation and characterization. We would like to thank Yiannis Gatzonis for his prior work on linear PHIC and for the data used in Figure 15.

## References and Notes

(1) de Gennes, P. G. *Scaling Concepts in Polymer Physics*; Cornell University Press: Ithaca, NY, 1979.
(2) Ferry, J. D. *Viscoelastic Properties of Polymers*, 3rd ed.; Wiley: New York, 1980.
(3) Doi, M.; Edwards, S. F. *The Theory of Polymer Dynamics*; Clarendon Press: Oxford, England, 1986.
(4) Sato, T.; Teramato, A. *Macromolecules* **1991**, *24*, 193.
(5) Larson, R. G. *Constitutive Equations for Polymer Melts and Solutions*; Butterworths: Boston, MA, 1988.
(6) Kratky, O.; Porod, G. *Recl. Trav. Chim. Pays-Bas* **1949**, *68*, 1106.
(7) Fuller, G. G. *Optical Rheometry of Complex Fluids*; Oxford University Press: Oxford, England, 1995.
(8) Johnson, S. J.; Frattini, P. L.; Fuller, G. G. *J. Colloid Interface Sci.* **1985**, *104*, 440.
(9) Onuki, A.; Doi, M. *J. Chem. Phys.* **1985**, *85*, 1190−1197.
(10) Fuller, G. G. *Annu. Rev. Fluid Mech.* **1990**, *22*, 387.

(11) Itou, T.; Chikiri, H.; Teramato, A.; Aharoni, S. M. *Polym. J.* **1988**, *20*, 143.
(12) Keep, G. T.; Pecora, R. *Macromolecules* **1988**, *21*, 817.
(13) Rubingh, D. N. Yu, H. *Macromolecules* **1976**, *9*, 681.
(14) Murakami, H.; Norisuye, T.; Fujita, H. *Macromolecules* **1980**, *13*, 145.
(15) Yu, M.; Liu, Q. *Macromolecules* **1996**, *29*, 6928.
(16) Gatzonis, Y.; Siddiquee, S. K.; van Egmond, J. W. *Macromolecules* **1997**, *30*, 7253.
(17) Wang, H.; Du Pre, D. B. *J. Chem. Phys.* **1991**, *96*, 1523.
(18) Yang, I. K.; Shine A. D. *J. Rheol.* **1992**, *36*, 1079.
(19) Berger, M. N.; Tidswell, B. M. *J. Polym. Sci., Polym. Symp.* **1973**, *42*, 1063.
(20) Conio, G.; Bianchi, E.; Cifferri, A.; Krigbaum, W. R. *Macromolecules* **1984**, *17*, 856.
(21) Kuwata, M.; Murakami, H.; Norisuye, T.; Fujita, H. *Macromolecules* **1984**, *17*, 2731.
(22) Fulmer, A. W.; Bensbasat, J. A.; Bloomfield, V. A. *Biopolymers* **1981**, *20*, 1147.
(23) Ferrari, M. E.; Bloomfield, V. A. *Macromolecules* **1992**, *25*, 5266.
(24) Weissenburg, P.; Odijk, T.; Cirkel, P.; Mandel, M. *Macromolecules* **1995**, *28*, 2315.
(25) Richtering, W.; Gleim, W.; Burchard, W. *Macromolecules* **1992**, *25*, 3795.
(26) Petekidis, G.; Vlassopoulos, D.; Fytas, G.; Kountourakis, N. *Macromolecules* **1997**, *30*, 919.
(27) Van Egmond, J. W.; Fuller, G. G. *Macromolecules* **1993**, *26*, 7182.
(28) Yamakawa, H. *Modern Theory of Polymer Solutions*; Harper & Row: New York, 1971.
(29) Tsetkov, V. N. *Rigid-Chain Polymers*; Plenum Press: New York, 1989.
(30) Takada, Y.; Sato, T.; Teramoto, A. *Macromolecules* **1991**, *24*, 6215.
(31) Chow, A. W.; Fuller, G. G.; Wallace, D. G.; Madri, J. A. *Macromolecules* **1985**, *18*, 786.
(32) Mansfield, M. L.; Stockmayer, W. H. *Macromolecules* **1980**, *13*, 1714.
(33) Doi, M. *J. Polym. Sci., Polym. Symp.* **1985**, *73*, 93.
(34) Hoff, S. M. Ph.D. Thesis, University of California, Berkeley, CA, 1997.
(35) Goodwin, A.; Novak, B. M. *Macromolecules* **1994**, *27*, 5520.
(36) Wyatt, P. J. *Anal. Chim. Acta* **1993**, *272*, 1.
(37) Schneider, N. S.; Furusaki, S.; Lenz, R. W. *J. Polym. Sci. A* **1965**, *3*, 933.
(38) Cook, R.; Johnson, R. D.; Wade, C. G.; O'Leary, D. J.; Munoz, B.; Green, M. M. *Macromolecules* **1990**, *23*, 3454.

MA971236Z